Analysis of Pulsed-laser Plasmon-enhanced Photothermal Energy Transfer with Applications

Fatema Alali[1], Ioannis Karampelas[2], Young Hwa Kim[1] and Edward P. Furlani[1,2]

[1]Dept. of Electrical Engineering, [2]Dept. of Chemical and Biological Engineering,
University at Buffalo SUNY, NY 14260, Office: (716) 645-1567 Fax: (716) 645-3822, faalali@buffalo.edu

ABSTRACT

We use computational models to investigate fundamental photothermal effects associated with nanosecond-pulsed, laser-heated colloidal metallic nanoparticles. We simulate energy conversion within gold nanoparticles at plasmon resonance, heat transfer from the particle to the surrounding fluid and phase change of the fluid leading to homogenous bubble nucleation. We consider various nanoparticle geometries including spheres, rods and tori. Our analysis demonstrates that nanotori or nanorings provide more efficient heating than nanorods due to their relatively high absorption at random orientations. We also show that process parameters such as the laser intensity, incident wavelength, pulse duration and shape of the nanoparticles can be tuned to optimize the photothermal process. In addition, we consider multi-particle systems and demonstrate effects of enhanced cooperative heating in such systems. Finally, we discuss the application of plasmon enhanced photothermal therapy to the destruction of cancer cells.

Keywords: Localized surface plasmon resonance (LSPR), photothermal energy conversion, plasmonic-enhanced photothermal energy transfer, LSPR-induced optical absorption, pulsed-laser photothermal heating.

1 INTRODUCTION

The ability to control thermal energy at the nanoscale is finding increasing use in emerging applications in fields such as nanoparticle synthesis, imaging and medical therapy, among others [1, 2]. Laser-based plasmon-enhanced photothermal energy conversion is of particular interest because it enables efficient heating with unprecedented (subwavelength) spatial resolution. In this approach, a pulsed laser is used to heat metalic nanostructures at their plasmon resonant frequency, which results in a peak absorption of incident photons and highly localized field enhancement [3]. In addition to enabling efficient nanoscale heating from a remote source, the optimal (resonant) wavelength for heating can be tuned within the ultraviolet through near-infrared spectrum using different shaped particles [4]. The plasmon resonance and associated absorption spectrum are well investigated both analytically and numerically for several nanoparticle geometries (i.e. nanospheres, nanorods, and nanoshells) [6-11]. However, relatively little is known of the plasmon resonance of metallic nanotorus structures. An analytical approach has been used to study resonance for two different orientations of this geometry [5], i.e. with the plane of the torus parallel and perpendicular to the incident field polarization, respectively. It was shown that for the parallel orientation, the absorption spectrum of the torus exhibits two resonances: a low intensity high energy resonance, and a high intensity low energy one. In this paper we numerically investigate the low energy plasmon resonance and its corresponding absorption spectrum with the nanotorus at arbitrary orientations with respect to the incident polarization. Our results demonstrate that nanotori have a relatively high absorption efficiency over a broad range of orientations. We also investigate nanosecond-pulsed laser illumination of gold nanoparticles in fluid taking into account heating that leads to bubble nucleation. In this presentation, we discuss fundamental aspects of plasmon-enhanced photothermal heating along with its application to cancer therapy.

2 RESULTS AND DISCUSSION

We model laser-induced, plasmon-assisted photothermal effects using continuum level photonic and fluidic analysis. The photonic analysis is performed using computational electromagnetics and is used to predict photothermal energy conversion within the nanoparticles, i.e. the time-averaged power absorbed by a particle as a function of the intensity, wavelength and polarization of the incident light. Maximum power absorption occurs at the plasmon resonant wavelength, which depends on the size, geometry and optical properties of the particle. The absorbed power is converted into heat and thus the particle becomes a heat source within the fluid. As the particle heats up, thermal energy is transferred to the fluid and a vapor bubble will nucleate at the particle-fluid interface if the critical vaporization temperature of the fluid is reached. Once nucleated, a bubble will exhibit a dynamic behavior (expansion and collapse) that is a complex function of the heat and mass transfer at the bubble-fluid interface as well as the temperature and flow in the surrounding fluid. This is

simulated using computational fluid dynamic (CFD) analysis.

2.1 PHOTONIC SIMULATIONS

For the photonic analysis we use 3D full-wave time-harmonic field theory. We perform the numerical simulations using the finite element-based COMSOL RF solver (wwww.comsol.com). The computational domain for the nanotorus geometry is shown in Fig.1a [4].

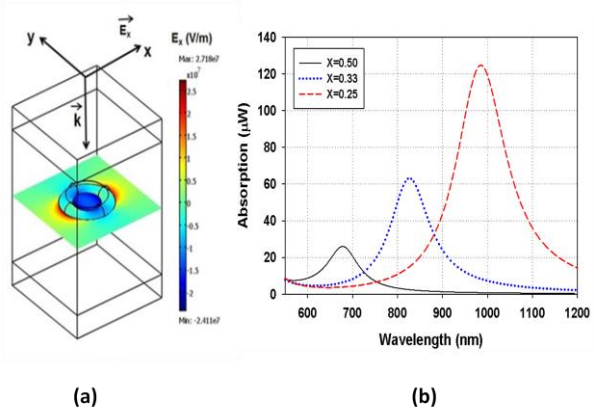

Figure 1. Photonic analysis for nanotorus: (a) computational domain and field analysis, (b) absorbed power vs. λ for different torus aspect ratios.

The torus is located at the origin of the computational domain as shown. The incident field is generated by a surface current (not shown) in the xy-plane at the top of the computational domain, which results in a TEM plane wave with the electric field polarized in the x-direction and the wave propagating downwards along the z- axis as indicated by the **k** vector [12, 13]. The permittivity of gold at optical frequencies is predicted using the following expression,

$$\varepsilon_{r,Au} = \varepsilon_{\infty} - \frac{1}{\lambda_p^2\left(\frac{1}{\lambda^2} - i\frac{1}{\gamma_p \lambda}\right)} + \sum_n \frac{A_n}{\lambda_n}\left[\frac{e^{i\phi_n}}{\left(\frac{1}{\lambda_n} - \frac{1}{\lambda} + i\frac{1}{\gamma_n}\right)} + \frac{e^{-i\phi_n}}{\left(\frac{1}{\lambda_n} + \frac{1}{\lambda} - i\frac{1}{\gamma_n}\right)}\right] \quad (1)$$

The parameters for this equation can be found in the literature [14]. It is instructive to investigate the absorption spectra of nanotori with different geometric aspect ratios. Here, we consider three different tori, each having a minor radius of r=10nm but with different major radii of R= 20nm, 30nm, and 40nm, respectively. This corresponds to three different aspect ratios X = r/R of 0.5, 0.33 and 0.25. The absorption spectra of the three nano tori with their plane parallel to the incident polarization are shown in Fig. 1b. Note that the absorption spectrum is red-shifts and has a narrower and more pronounced peak as the aspect ratio decreases (i.e. thinner torus). It is instructive to study the absorption spectra of a torus at different orientations and to compare this with the corresponding absorption by nanorods (Fig. 2).

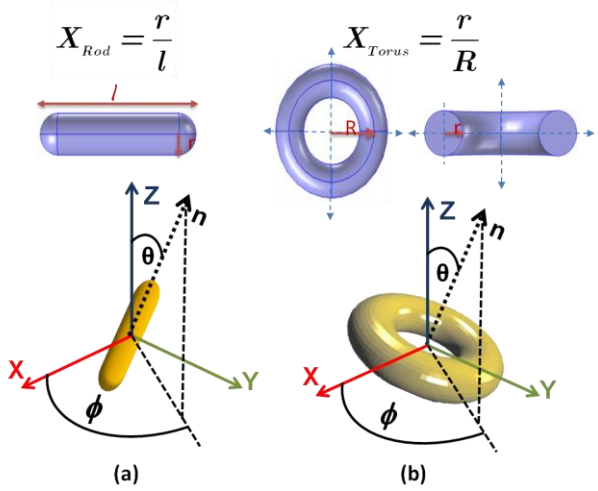

Figure 2. The aspect ratio and orientation angles defined by the ones of spherical coordinate's θ and φ for (a) nano rod and (b) nano torus.

It is well known that a gold nanorod exhibits maximum absorption when its major axis is aligned with the polarization of the incident light (parallel polarization) at the longitudinal plasmon resonant wavelength. However, as the nanorod rotates away from this orientation, the absorption decays significantly as shown in Fig. 3a.

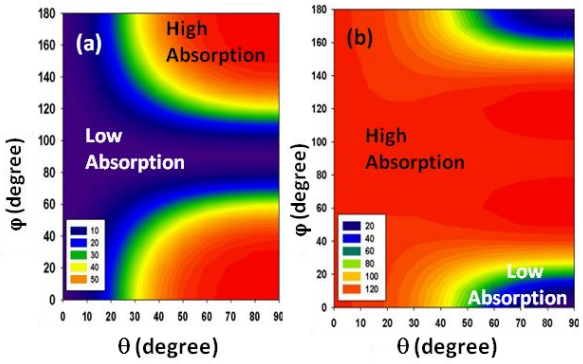

Figure 3. NIR resonance absorption at any random orientation as a function in θ and φ for (a) nano rod with aspect ratio of 0.28 at λ= 770nm and (b) nano torus with X=0.25 at λ=986nm.The chosen resonance wavelengths are the ones of parallel orientation.

Specifically, this plot shows contours of absorbed power as a function of the angles θ and ϕ that define the orientation of the axis of the nanorod (Fig 2a). Note that high absorption occurs when the nanorod is aligned with the x-axis (incident polarization), i.e. θ = 90° and ϕ = 0°, but drops off as it rotates away from this orientation and

researches a minimum when its axis is aligned orthogonal to the polarization, i.e. when $\theta = 0°$ and $\phi = 0°$ (aligned along the z-axis) or when $\theta = 90°$ and $\phi = 90°$ (aligned along the y-axis). This is due to a reduction of the induced current density at different orientations. Hence, for NIR resonance, high absorption in a nanorod is restricted to (near) parallel polarized orientations. This is in sharp contrast to the nanotorus wherein relatively high absorption is achieved throughout a wide range of possible orientations (Fig. 3b). In fact, our results show that peak absorption in a nanotorus occurs at orientations offset from parallel alignment. This is due to the excitation of more complex plasmon modes within the torus that give rise to higher current densities and thus more power dissipation. This higher absorption over an extended range of orientations is potentially useful for applications involving photothermal heating of a colloid of nanoparticles wherein one would expect a random distribution of particle orientations. One such application involves the use of metallic nanoparticles for photothermal cancer therapy as described below. In this application metallic nanoparticles are utilized to target cancer cells and are transported into the interior of the cell via magnetic fields. Once a collection of such particles are inside the cell, they can be heated with a pulsed-laser to cause bubble generation, which in turn can destroy the cell by rupturing its membrane. In the following section, we discuss the use of CFD analysis to predict the heating of the particles and bubble formation.

2.2 FLUIDIC SIMULATIONS

Once the absorption spectra of a plasmonic nanoparticle is known, a CFD analysis can be performed to determine viable parameters for the pulsed-laser heating required to heat the particle in a controlled fashion and, if desired, to achieve bubble nucleation (vaporization) with or without destroying (melting) it [4]. The first step in this study involves a preliminary thermal analysis to identify a viable power and pulse duration required to increase the temperature of the particle from the ambient temperature to the supercritical temperature at which vaporization occurs. We demonstrate this analysis using a nanotorus with dimensions as defined above, i.e. minor and major radii of r=10nm and R= 30nm, respectively (X = 0.33). We calculate the temperature of the torus during heating for a range of power levels and pulse durations. The latter are chosen to be from 2 to5 ns. Once this analysis is complete, the results are used in a subsequent parametric CFD-based study that takes into account phase change leading to bubble nucleation in order to determine viable power levels and pulse durations that are sufficient to nucleate a sustained bubble without destroying the nanotorus. In this particular case, it is found that an adequate power for nucleation is 72.8 mW, with pulse duration of 4.1 ns. Given these values and the results of the photonic analysis (Fig. 1b) we determined that a laser operating at the plasmon resonant wavelength of λ=828 nm with an irradiance of I_{inc}= 19.27 mW μm^{-2} is sufficient to generate and sustain a bubble without melting the nanotorus. The fluidic analysis for this power and pulse duration is shown in Fig. 4. This plot shows the temperature of the torus throughout the photothermal process along with corresponding images of the bubble dynamics. Initially the torus is at ambient temperature. After 0.2 ns it is illuminated and its temperature begins to rise. During the first3.4 ns of heating, its temperature gradually increases (Fig. 4a) to the superheat temperature, at which point a bubble is nucleated around it. Once this occurs the torus is surrounded by vapor and its temperature increases rapidly as it is still absorbing energy. It reaches a peak temperature of approximately 1000 K, which occurs at the end of the heat pulse (4.1 ns), at which point it is completely surrounded by vapor (Fig. 4b). As soon as the bubble has nucleated, it expands and reaches its maximum size at 5.4 ns after the onset of heating. At this time the bubble has a spherical shape, approximately 80 nm in radius. An interesting feature of this process is the residue of an isolated drop of heated fluid that forms in the middle of the torus during the bubble expansion as seen in Fig. 4c. Eventually, 8.7 ns after the onset of heating, the nanobubble collapses, bringing fluid back in contact with the torus (Fig. 4d). Consequently, it slowly cools to the ambient temperature as more of the fluid comes in contact with it (Fig. 4e). It is instructive to

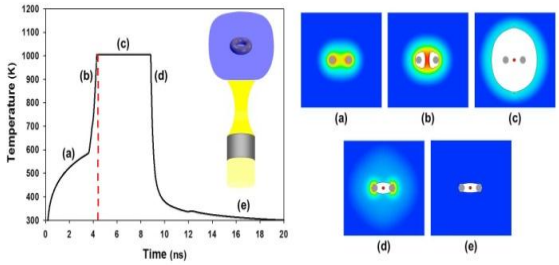

Figure 4. Pulsed laser illumination of Au nanotorus in fluid. Photothermal heat cycle: (a) initial heating (to red dotted line), (b) bubble formation, (c) bubble (maximum size), (d) bubble collapse, (e) cooling.

note that the capillary force that acts to collapse the bubble is relatively weak because of the relatively large radius of curvature that defines the fluid–vapor interface as it gets closer to the torus. Thus, the nanobubble requires a substantial amount of time to completely collapse, compared to other geometries [4].

The photonic and fluidic simulations described in this and the previous sections are useful for the rational design and optimization of photothermal applications. We discuss one such application involving cancer treatment in the next section.

2.3 PLASMON-ENHANCED PHOTOTHERMAL CANCER THERAPY

Photothermal cancer therapy is an emerging field and there is currently a proliferation of new therapeutic modalities due in part to rapid advances in the development of multifunctional nanoparticles that facilitate the detection, diagnosis and treatment of malignant tissue. An example of such a particle that we have recently developed is a novel bioactive magneto-plasmonic nanoplatform (Fig. 5a), that can be used to target cancer cells and provide high photothermal response and related cytotoxicity using NIR

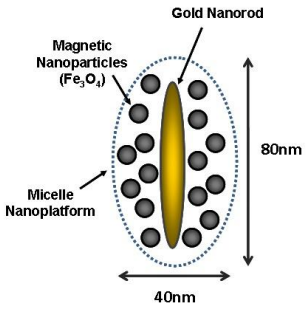

(a)

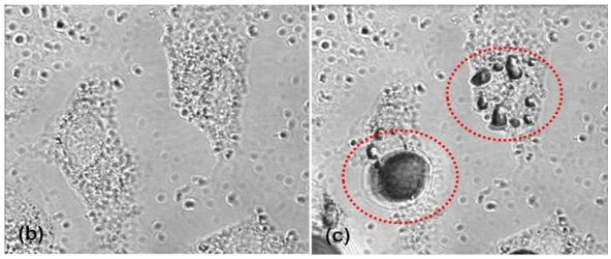

Figure 5. (a) magneto-plasmonic nanoplatform (MPNP), (b) HeLa cells containing MPNPs before illumination, (c) HeLa cells containing field-aggregated MPNPs with plasmon-enhanced bubbles (circled in red) generated by pulsed laser (λ= 780 nm) illumination.

illumination [15]. Specifically, this is a polymeric micelle-based magneto-structure that contains a 10x60 nm gold nanorod surrounded by 10-20 Fe_3O_4 particles (~15 nm). The nanoplatform is functionalized to promote uptake by HeLa cells. Following uptake, the nanoplatforms are illuminated with a femtosecond-pulsed NIR laser, which causes photothermal destruction of cells due to laser-induced plasmon-enhanced heating and bubble generation as shown in Figs. 3b and 3c. Preliminary results demonstrate that magnetic field-induced aggregation of the nanoplatforms dramatically enhances the ability to heat and destroy targeted cells. Based on the modeling described above, nanoplatforms with embedded Au nanotori or nanorings would provide even more effective photothermal therapy because of their ability to absorb energy over a broader range of orientations.

3 CONCLUSIONS

We have discussed advantages of using plasmonic particles for photothermal applications and have shown that the energy conversion of such particles is a sensitive function of their geometry and orientation. We have demonstrated the use of computational electromagnetic and fluid dynamic analysis to study pulsed-laser heating of colloidal plasmonic nanoparticles including phase change leading to bubble generation. We have used the modeling to determine power levels and pulse durations that are sufficient to generate a desired bubble dynamics, while avoiding damage to the particle through excessive heating. We have also showed that the plasmon resonance of nanotori can be tuned to NIR frequencies by adjusting their aspect ratio. Compared to nanorods, they have higher absorption over a broader range of orientations. Thus, gold nanotori or nanorings hold potential for more effective and deeper tissue photothermal tumor therapy.

REFERENCES

[1] West, J. L. and Halas N. J., Current Opinion in Biotechnology **11**(2): 215-217, 2000.

[2] Pitsillides, C.M. *et. al.*, Biophysics Journal. **84:** 4023-4032, 2003.

[3] Roper, D.K., W. Ahn, Hoepfner, M., J. Phys. Chem. C **111**(9): 3636-3641, 2007.

[4] Furlani, E. P., Karampelas I. H., et al. Lab on a Chip **12**(19): 3707-3719, 2012.

[5] C. M. Dutta, T. A. Ali, D. W. Brandl, T. Park and P. Nordlander, J. Phys. **129**, 084706, 2008.

[6] O. Ekici, R. K. Harrison, N. J. Durr, D. S. Eversole, M. Lee and A. Ben-Yakar, Journal of Physics D-Applied Physics, 2008, **41**.

[7] E. Hao, G. Schatz and J. Hupp, J. Fluoresc., 2004, **14**, 331–341.

[8] C. Sonnichsen, T. Franzl, T. Wilk, G. von Plessen, J. Feldmann, O.Wilson and P. Mulvaney, Phys. Rev. Lett., 2002, **88**, 077402.

[9] E. Hao and G. Schatz, J. Chem. Phys., 2004, **120**, 357–366.

[10] M. Hu, J. Chen, Z. Li, L. Au, G. V. Hartland, X. Li, M. Marqueze and Y. Xia. Chem. Soc. Rev., 2006, **35**, 1084–1094.

[11] D. W. Brandl and P. Nordlander. J. Chem. Phys. **126**, 144708 (2007); doi: 10.1063/1.2717167

[12] E. P. Furlani and A. Baev, Phys. Rev. E, **79,** 2009.

[13] E. P. Furlani and A. Baev, J. Modern Optics, **56**, 523-529, 2009.

[14] P. G. Etchegoin, E. C. Le Ru and M. Meyer, J. Chem. Phys., **127**, 2007.

[15] T. Y. Ohulchanskyy, A. Kopwitthaya, M. Jeon, E. P. Furlani, C. Kim and P. N. Prasad, submitted to Nanomedicine, first revision under review, 2013.